

LARGE EDDY SIMULATION OF MIXED JET IN CROSSFLOW AT LOW REYNOLDS NUMBER

Jianlong Chang^{1,2}, †Guoqing Zhang^{2} and Xudong Shao³

¹College of Mechatronic Engineering, North University of China

²School of Aerospace Engineering, Beijing Institute of Technology

³Beijing Institute of Space Systems Engineering

*Presenting author: changjianlong1989@126.com

†Corresponding author: zhanggq@bit.edu.cn

Abstract: Large eddy simulation for a jet in crossflow at very low Reynolds number ($Re=100$) is performed for different jet-to-crossflow velocity ratios (r) ranging from 1 to 4.5, and the corresponding streamlines, vortex characters and interaction between the vortices have been analyzed. The results show that the streamlines for the jet in crossflow are closely related to the velocity ratios. The evolution of three-dimensional vorticity for displaying the formation of large-scale vortices has also been investigated. Near the nozzle of the jet, the stable mixed vortices including the counter-rotating vortex pair (CRVP), the horseshoe-vortex (HSV), the wake vortices (WV), the upright-vortices (UV) and the ring-like vortices come into being. The presence of the CRVP and RLV structures can maintain a quite long distance even to the flow exits at lower velocity ratio. However, the RLV are in destruction soon at larger velocity ratios under the interaction for the mixed jet in crossflow. Vortex evolution at velocity ratio $r=1.5$ have been displayed to explain the mechanism of the regular vortex under the interaction of UV and WV. The velocity streamlines have been obtained computationally and analyzed in details.

Keywords: jet in crossflow (JICF); large eddy simulation (LES); vortex interaction; vortex.

1. Introduction

A jet in crossflow (JICF) is an important flow phenomenon that is defined as the flow field where a jet of fluid enters and interacts with a crossflowing fluid [Muppidi (2007)]. There are various applications in the engineering problems such as the aerodynamic flow control, film cooling of turbines and combustors, control of separated flows over an airfoil, industrial mixing, and pollutant dispersion from effluent stacks [Lim (2006)].

In the past 70 years, numbers of experimental and computational research for JICF have been conducted. These researches mainly focus on the development and evolution of large-scale vortex structures, trajectory and other related flow phenomena. The interaction between the jet and the crossflow can generate the coherent vortex structures: the counter-rotating vortex pair (CRVP), the horseshoe-vortex (HSV), the wake vortices (WV), the upright-vortices (UV) and the ring-like vortices (RLV) [Cárdenas (2007)]. Fig. 1 has shown a side view of the corresponding vortex in the flow field. An experimental investigation on the

effects of jet velocity profiles on the flow field of a round jet in cross-flow (JICF) using laser-induced fluorescence and digital particle-image velocimetry techniques (DPIV) have been conducted [New (2006)] in 2006. The results had shown that the parabolic JICF not only can exhibit a faster velocity recovery, it can also register a higher magnitude of the peak average vorticity. The establishment [Camussi (2002)] of different behaviours at various velocity ratios is interpreted physically as an effect of the Reynolds number of the jet. This means that the Reynolds number has an essential effect on the destabilization mechanisms for the formation of the mixed vortex. The CRVP undulates in the turbulent flow and interacts with the intermittent wake vortices which in turn interact with the boundary layer and the vortices therein [Salewski (2008)].

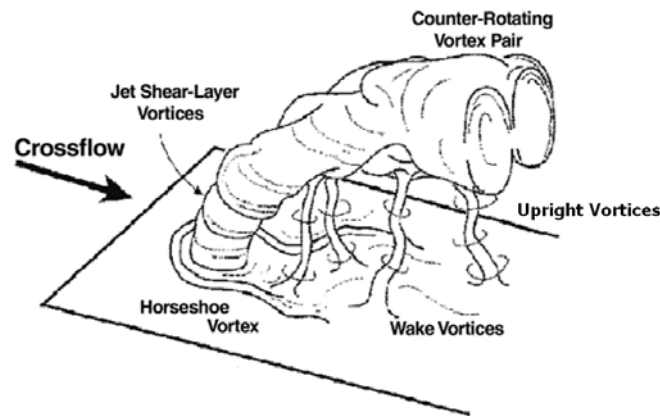


Fig. 1 Vortex Structures of a JICF [Jouhaud (2007)]

A new model [Mashayek (2011)] for atomization of a turbulent liquid jet in a subsonic crossflow had been developed. The corresponding results had shown that the droplets stripping apart from the jet body can make a great contribution to the formation of the vortical structures along the wake of the jet. It was also shown that the spreading of the jet into a sheetlike shape strengthened the extent of the vortical structures in the JICF, which will affect the droplet dynamics downstream of the jet. The problem of the proper choice of the turbulent Schmidt number in the Reynolds-averaged Navier-Stokes (RANS) jet in crossflow mixing simulations had been summarized [Ivanova (2013)]. The mainly conclusion was that the turbulent Schmidt numbers ranging from 0.2~0.3 used in JICF simulations for obtaining the optimal mixing predictions were not in agreement with the physical reality. More accurate prediction of mixing in JICF is significantly important to the development of combustion systems. The turbulent mixing of a jet in crossflow performed at the Reynolds number of 6930 by using the large eddy simulation method [Esmaeili (2015)]. The velocity profile for the jet pulsation substantially affected the JICF structures, and relatively low Strouhal numbers ranging from 0.0075 to 0.05 can develop an optimal condition for mixing, entrainment and penetration in the corresponding JICF. The effects of pulsing of high-speed subsonic jets ($Ma=0.47\sim 0.77$) on mixing and jet trajectory in turbulent subsonic crossflows by using large-eddy simulation had been investigated [Srinivasan (2012)]. The regime of pulsed JICF had shown both the similarities and differences to the earlier experimental work. At the larger Strouhal number, the vortex interaction will still increase. However, the vortex ring will

be broken down in a relative short time, resulting in reduced penetration at a larger Strouhal number.

One leading parameter determining the development and evolution of large-scale vortex structures in JICF is the velocity ratio r [Yuan (1999)], if the densities in the jet and the crossflow are the same, r can be defined as:

$$r = \frac{V_{jet}}{V_{crossflow}} \quad (1)$$

otherwise, the effective velocity ratio r can be obtained by the square root of the momentum flux ratio as [Gutmark (1999)].

$$r = \sqrt{\frac{(\rho V^2)_{jet}}{(\rho V^2)_{crossflow}}} \quad (2)$$

The simulation and analysis for a jet in crossflow at very low Reynolds number ($Re=100$) will be performed for different jet-to-crossflow velocity ratios (r) ranging from 1 to 4.5.

2. Numerical methods and flow configuration

2.1. Numerical methods

At present research, the large eddy simulation (LES) has been adopted, because the LES turbulence model is different from Reynolds Averaged Navier-Stokes Equation (RANS) and Direct Numerical Simulation (DNS). The aim of the LES is to resolve the large scale of turbulence, and the smaller ones are modeled based on the universality. By filtering process in the large eddy simulation, the vortices less than a certain scale are filtered from the flow field, large eddy is calculated firstly. Then the solution of small eddy by solving additional equation will be obtained. Consequently, LES is more suitable for industrial configurations, in which large scales are known to be essential. In the case of the JICF, the unsteady behavior of the various flow structures is expected to be more important, the unsteady LES approach that provides spatiotemporal resolution should be used [Jouhaud (2007)].

In the LES method, the whole flow will be divided into large-scale eddy and small-scale eddy. Basic equations of LES are obtained after filtering Navier-Stokes equation and the continuity equation [Chen (2010)]:

$$\frac{\partial(\overline{\rho u_i})}{\partial t} + \frac{\partial(\overline{\rho u_i u_j})}{\partial x_j} = -\frac{\partial \overline{p}}{\partial x_i} + \frac{\partial}{\partial x_j} \left(\mu \frac{\partial \overline{u_i}}{\partial x_j} - \frac{\partial \tau_{ij}}{\partial x_j} \right) \quad (3)$$

$$\frac{\partial \overline{\rho}}{\partial t} + \frac{\partial(\overline{\rho u_i})}{\partial x_i} = 0 \quad (4)$$

where ρ is the density of fluid, u_i and u_j are the velocity components, p is the pressure, μ is the kinematic viscosity coefficient, the variables of formula with an overline are the field variables filtered.

Component of subgrid-stress tensor (SGS) is obtained as $\overline{\tau_{ij}} = -\rho(\overline{u_i u_j} - \overline{u_i} \overline{u_j})$. And u_i is defined as $u_i = \overline{u_i} + u'_i$, therefore the SGS can be decomposed into three parts:

$$\begin{aligned} \tau_{ij} &= \overline{u_i u_j} - \overline{u_i} \overline{u_j} = \overline{(\overline{u_i} + u'_i)(\overline{u_j} + u'_j)} - \overline{u_i} \overline{u_j} \\ &= \overline{\overline{u_i} \overline{u_j}} - \overline{u_i} \overline{u_j} + \overline{u'_i \overline{u_j}} + \overline{\overline{u_i} u'_j} + \overline{u'_i u'_j} = L_{ij} + C_{ij} + R_{ij} \end{aligned} \quad (5)$$

where, L_{ij} is Leonard stress of the SGS, which can be obtained by $L_{ij} = \overline{\overline{u_i} \overline{u_j}} - \overline{u_i} \overline{u_j}$. $C_{ij} = \overline{\overline{u_i} u'_j} + \overline{u'_i \overline{u_j}}$, and it is named cross stress of the SGS. R_{ij} captured by $R_{ij} = \overline{u'_i u'_j}$ represents the Reynold stress of the SGS. L_{ij} shows the motion effect among the solvable large eddy, C_{ij} stands for the motion effect between the solvable large eddy and the unsolvable small eddy, and R_{ij} is the interaction among the unsolvable small eddy, respectively.

Based on the assumption of Boussinesq, the relationship between $\overline{\tau_{ij}}$ and $\overline{S_{ij}}$ can be expressed as:

$$\overline{\tau_{ij}} - \frac{1}{3} \delta_{ij} \overline{\tau_{kk}} = -2\mu_T \overline{S_{ij}} \quad (6)$$

where μ_T is turbulent viscosity, δ_{ij} is Kroneker symbol, $\overline{S_{ij}}$ is strain rate tensor after filtering,

$$\overline{S_{ij}} = \frac{1}{2} \left(\frac{\partial \overline{u_i}}{\partial x_j} + \frac{\partial \overline{u_j}}{\partial x_i} \right) \quad (7)$$

Turbulent viscosity μ_T can be configured as product between length scale l and velocity scale q . By assuming that the magnitude of small-scale is in equilibrium, length scale and velocity scale can be defined as $l = C_s \overline{\Delta}$, $q = \overline{\Delta} |\overline{\mathbf{S}}|$, then the turbulent viscosity μ_T can be expressed as:

$$\mu_T = l^2 |\overline{\mathbf{S}}| \quad (8)$$

where C_s is constant of Smagorinsky, the approximation of the constant is

$$C_s \approx \frac{1}{\pi} \left(\frac{3C_k}{2} \right)^{-3/4} \quad (9)$$

The value measured in the atmosphere for Kolmogorov constant is 1.4, thereby $C_s \approx 0.18$. However, the value of C_s is usually taken as 0.1 in practical application. $\overline{\Delta}$ is the scale of grid filter, and it is obtained by $\overline{\Delta} = (\Delta x \Delta y \Delta z)^{1/3}$. For unstructured grids, $\overline{\Delta}$ could be acquired by extracting a cube root for the unit volume. $\overline{\mathbf{S}}$ can be captured by

$$|\overline{\mathbf{S}}| = \sqrt{2 \overline{S_{ij}} \overline{S_{ij}}} \quad (10)$$

2.2. Flow configuration and grid distribution

Fig.2 shows the flow configuration and the size of the computational domain. The flow region is rectangular, the length, breadth and height are $65D \times 20D \times 16D$. The jet channel is circular and Reynolds number of the fluid is 100, D presents the diameter of round jet. The structured grids will be adopted in the calculation, and the corresponding mesh have also been refined near the entrance of jet.

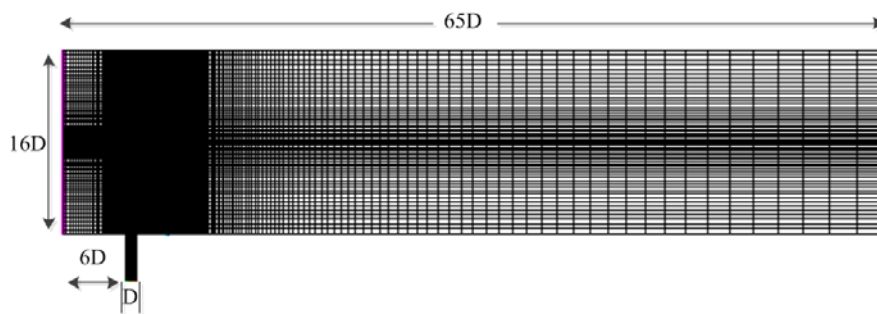


Fig. 2 View of the grid

3. Results and discussion

3.1. Time-averaged particle trajectory

The connection of the jet center has been defined as the time-averaged particle trajectory for the JICF. Fig.3 shows different trajectories obtained from the stream traces. These time-averaged particle trajectories show that by the action of the crossflow the jet is deflected downstream. In the proximity of the jet exit, it is noticed that the trajectories are almost vertical up to the main flow indicating that the ability of vertical penetration for the cases is about the dimension of the jet [Saha (2012)]. As shown in Fig.3, the jet has a larger kinetic energy and a stronger penetration compared with the crossflow near the nozzle, therefore the jet can quickly flow across the boundary layer. Once the jet reaches the crossflow in the flow channel, it will experience drastic exchange of energy and momentum, and penetration capability of the jet decreases leading to a deflected jet thereby. This phenomenon can produce more complex vortices, such as the counter-rotating vortex pair, upright vortex, vortex ring, horseshoe vortex and wake vortices, respectively.

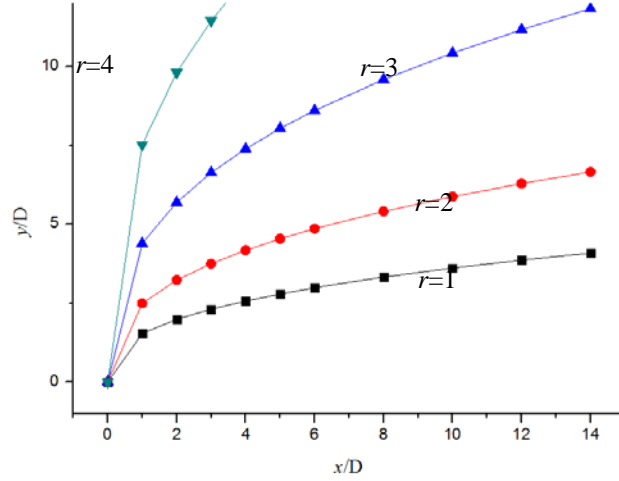


Fig. 3 Time-averaged particle trajectories for the JICF

Comparison of various cases in Fig.3, it has revealed that the jet penetration is highest for the highest r and it is almost followed by velocity ratio r . The upstream for the inflow with boundary layer near the nozzle can generate more kinetic energy loss. This will result in the higher pressure gradient in the vertical direction which rises fluid upwards to a higher extent. Thereby, the more momentum loss, the deeper penetration of jet in crossflow will reach for a given jet profile.

The time-averaged particle trajectories in the JICF can be approximately expressed as [Chassaing (1974) and Camussi (2002)]:

$$y = A(x)^n \quad (11)$$

where y is the height of the jet penetration, x is the streamwise position. In the presented cases, the corresponding A and n are listed in Tab. 1. The studied cases in this paper have shown a good agreement with the experiment results (Camussi 2002) within 5% error. This demonstrates that the large eddy simulation has higher accuracy.

Table 1 Coefficient A and n

veolicity ratio	A	A (Camussi 2002)	relative error of A (%)	n	n (Camussi 2002)	relative error of n (%)
1	1.5377	1.5962	3.66%	0.3708	0.39	4.92%
2	2.4926	2.5158	0.92%	0.3723	0.39	4.54%
3	4.3904	4.566	3.85%	0.3755	0.39	3.72%
4	7.5213	7.865	4.37%	0.3821	0.39	2.03%

3.2. Evolution of three-dimensional vortex

Fig.4 is an overall view of vortex structure in JICF at Reynolds number $Re=100$ with a velocity ratio $r=1.5$. It is apparent that the spatial evolution for large-scale such as CRVP and RLV can be clearly observed, the HSV, UV and WV have been also shown below the large scale vortices (CRVP and RLV). Near the nozzle, the CRVP and RLV have appeared due to

the action of shear layer. While once produced, the vortices will not immediately fall off, but stretch along the flow at a certain frequency. The CRVP and RLV generate a gradually rising in the interaction among the small scale vortices (HSV, UV and WV) and boundary layer. As shown in Fig.4(a), the vortices are generated near the nozzle, with the increasing distance from the entrance of the jet, scale and strength of vortex rings are enhancing (Fig.4(a)~(e)). With the further development of the JICF, the intensity of vortices will be evolved stronger, the CRVP and RLV start to fall at a certain time after deformation and distortion. The falling frequency of vortices is much faster than the formation. After completing the process of falling, the JICF will generate more stable CRVP far away from the nozzle (Fig.4(f)).

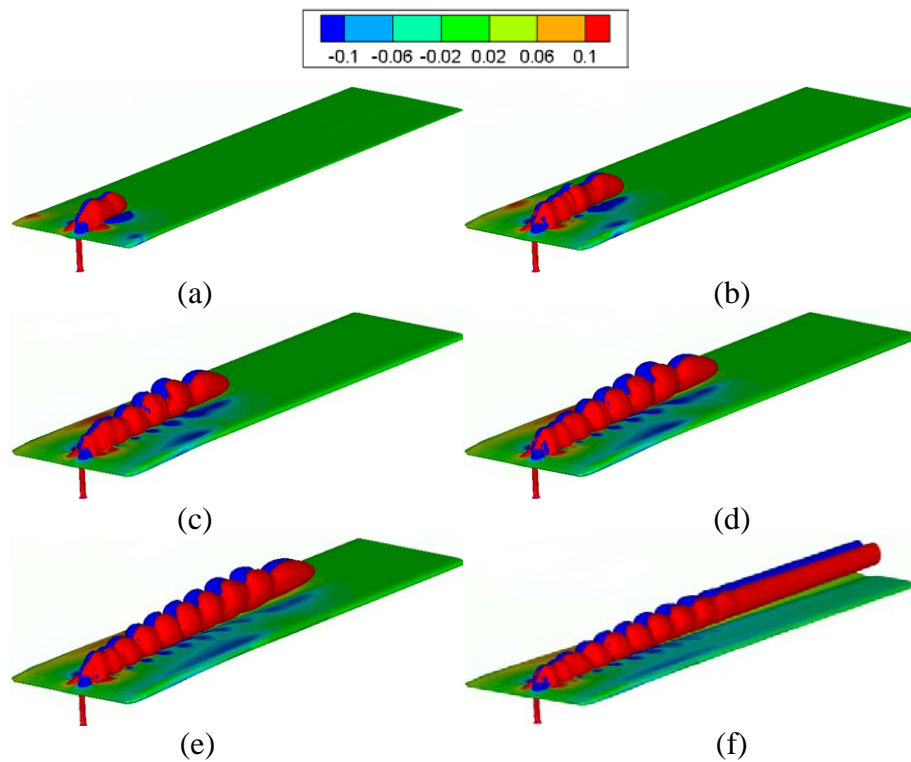


Fig. 4 Evolution of vorticity for JICF with a circle nozzle
(a) $t=1.9s$; (b) $t=3.74s$; (c) $t=6.24s$; (d) $t=7.8s$; (e) $t=9.86s$; (f) $t=15.72s$

3.3. Analysis of three-dimensional vorticity

After flowing into the crossflow, the jet will generate three processes under the interaction of the jet and crossflow: the initial phase, the curved phase and penetration phase. The JICF will make an access to the full development phase after shearing, wrapping and other effects. The small-scale structure in the jet core area surrounding is ongoing for stretch, rupture merged into the large scale vortices. The CRVP and RLV will be broken down into crossflow. Far away from the entrance, the previous vortices will gradually decline and evolve into CRVP at higher r .

The evolution and interactions for the vortices structures are significantly affected by the variations of velocity ratio. In particular, the vortex content of the CRVP and RLV are

analyzed, showing a vortex flow phenomena which strongly depends on r . The most important effect of r on the flow behavior is the changing of the CRVP and RLV structures.

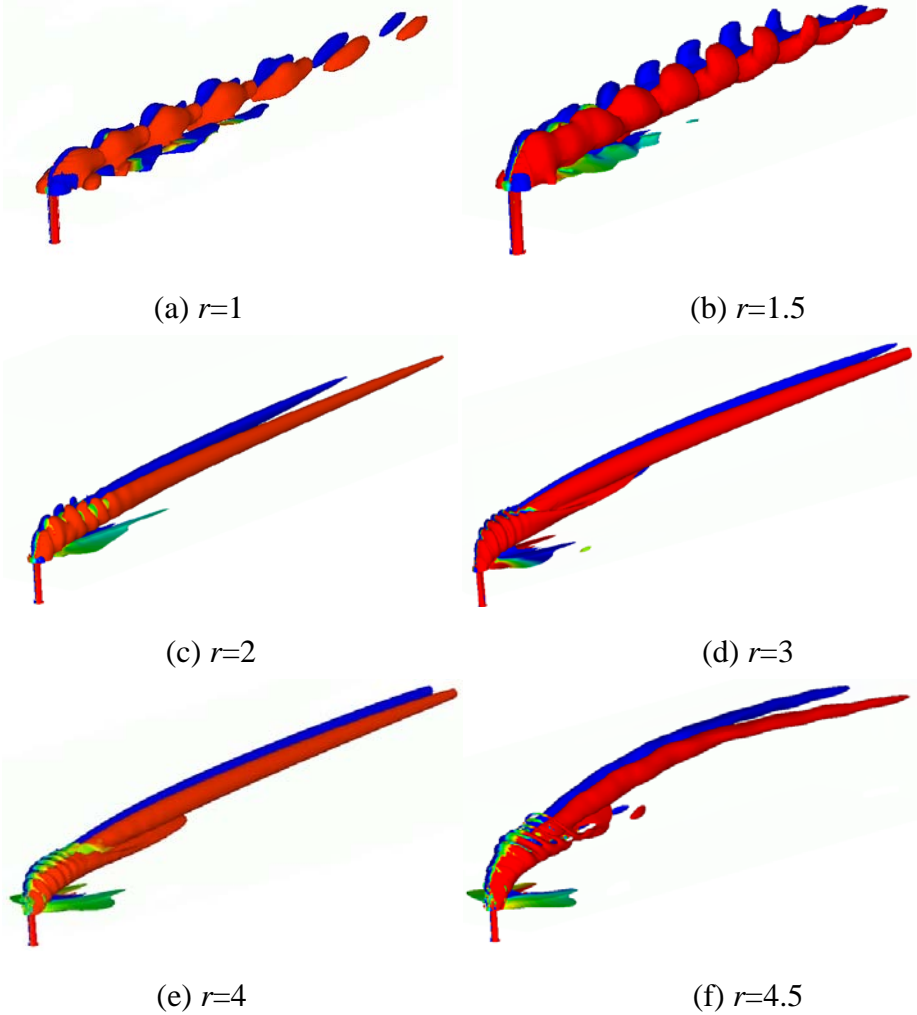


Fig. 5 Three-dimensional vorticity

As shown in Fig.5, the presence of CRVP and RLV structures can last quite a long distance even to the flow exits at lower velocity ratio (Fig.5(a) and (b)). The interval between CRVP and RLV is relatively large. However, when the velocity ratio becomes larger (Figs.5(c)~(f)), the RLV could only maintain a short distance. Forming frequency of RLV increases with the increasing velocity ratio r . While with the augment of velocity ratio, the jet kinetic energy increases, gap of the RLV near the nozzle will be generated closer, and the diameter for the RLV will become smaller. However, due to the strong interaction of the WV, HSV, UV, RLV and shear layer, the RLV will be destroyed soon.

3.4. Vortex Interaction

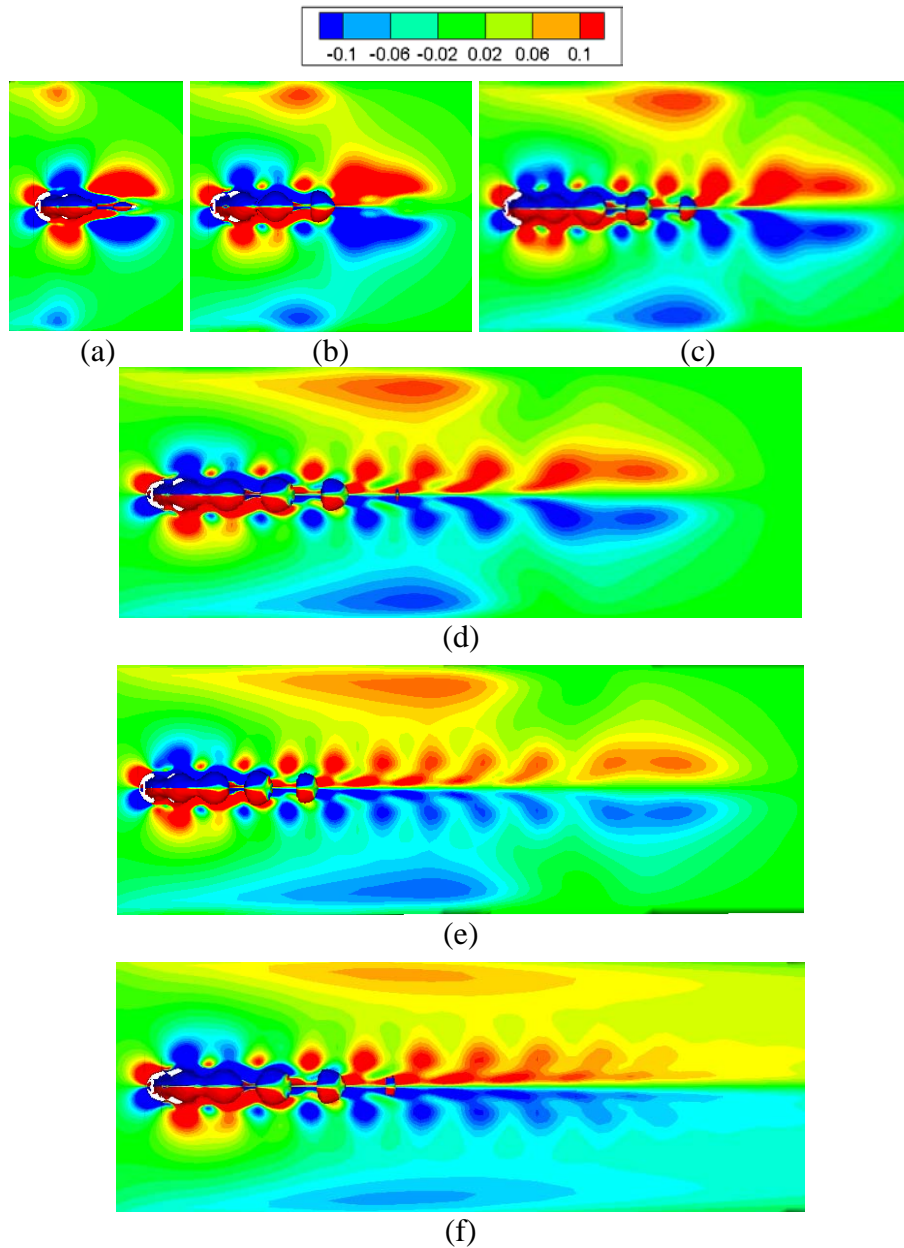


Fig. 6 Evolution for interaction of HSV, WV and UV at $r=1.5$
 (a) $t=1.9s$; (b) $t=3.74s$; (c) $t=6.24s$; (d) $t=7.8s$; (e) $t=9.86s$; (f) $t=15.72s$

It is essential to investigate the interaction of the WV, HSV, UV, RLV and shear layer, which is the main reason for the disappearing of the RLV. A scheme for clarifying this feature has been displayed in Fig.6, which has shown the evolution of interaction between the UV, HSV and WV at $r=1.5$. The formation of the HSV is near the nozzle (Fig.6(a)), which is seemed to show a fixed shape during the evolution. Once affected by UV in the initial phase, the HSV can generate a stable status through a period of development (Fig.6(a)~(f)). Since the HSV is formed earlier than the CRVP, the CRVP can only affect WV.

As shown in Fig.6, the most significant phenomenon is the evolving regular vortex, which can be attributed to the interaction between the UV and WV. From the outset, the core area of the jet is strongly influenced by the interaction between the boundary layer and the UV system, therefore, the jet is restrained which can result in lifting up from the jet core area. There is a clear exhibition about the flow of the oscillation along the direction of crossflow. The regular vortex will be generated below the CRVP and RLV under the interaction of the UV and WV. Due to the combined effect of the jet, boundary layer, the WV, HSV, UV in the jet core area, vortices including the regular vortices and large scale eddy will be soon decomposed to a series of shocking eddy wrapped into the wake zone (shown in Fig.6(f)) [Guan (2007)].

3.5.Spanwise Velocity Streamlines

As shown in Fig.7, the CRVP have been clearly generated based on different velocity ratios ($r=1\sim 4$) by adopting the spanwise velocity streamlines, which is formed due to the high velocity ratio. The annular area affected by the CRVP (marked with red circle) at lower velocity ratio has an approximately elliptical shape with a smaller acreage. The velocity stream is seemed to converge at one point above the CRVP. However, with the increasing the velocity ratio, the eccentricity for the annular area affected by CRVP is nearly generated at zero, which means that the shape of the annular area is almost in the circle shape. As a matter of course, the corresponding area is followed bigger by r .

When $r=1$ (Fig.7(a)), to be same to the other studied cases (Figs.7(b)~(d)), the relatively symmetric vortices pair have been formed at the upper boundary. However, the corresponding intensity of the crimping and winding for the formed vortices at low ratio ($r=1$) are much weaker than the other cases. In addition, the whole rotating region is also much more flat. As the velocity ratio further increases, the whole former formed vortex cores have begun to move up gradually (shown in Figs.7(b)~(d)). And the corresponding strength have also been boosted up. The whole vortex regions have become more circular and greater. When $r=4$ (shown in Fig.7(d)), the intensity and region of the formed vortices have reached the maximum value. The spanwise position for the vortex core has located nearly five times height compared with the lowest velocity ratio (shown in Fig.7(a)). Except this, as shown in Fig.7(d), the second vortices have also been induced by the formed CRVP at relatively higher velocity ratios ($r=4$). The higher velocity ratio got, the stronger second vortices can be obtained. And the corresponding position is also gradually moving up, which will be swallowed up by the CRVP ultimately at a certain downstream position.

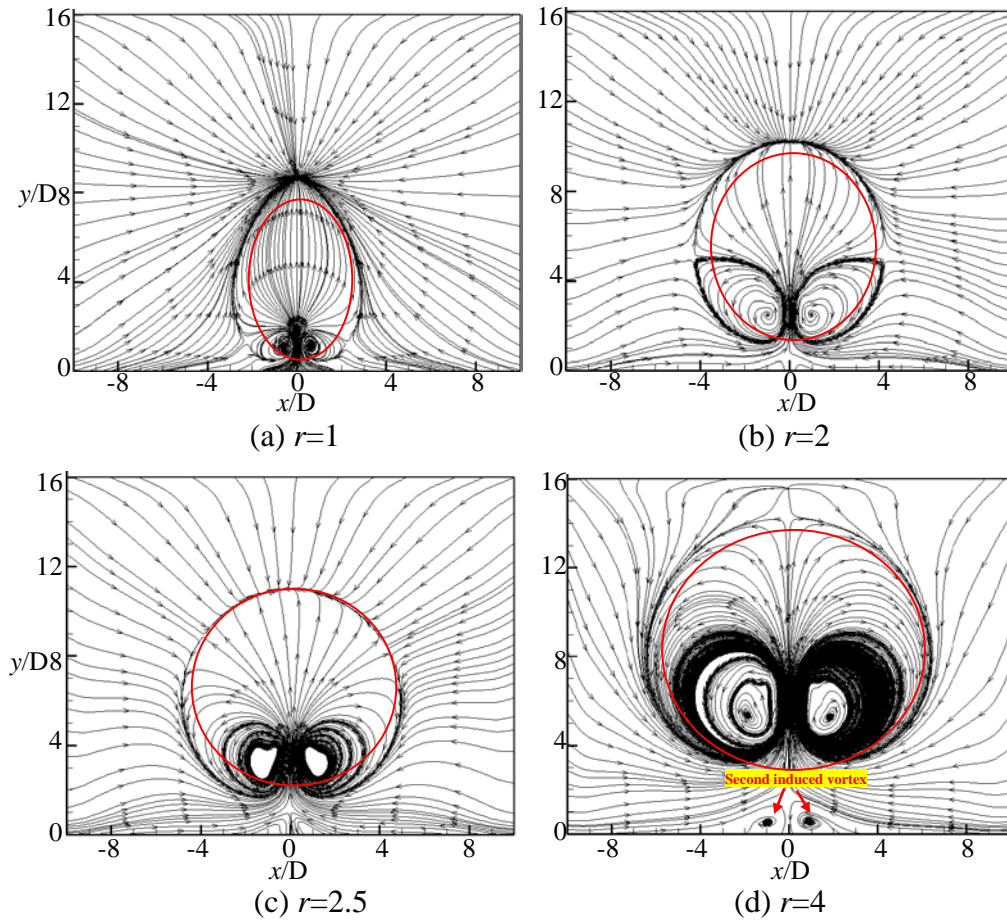


Fig. 7 The spanwise velocity streamlines for the JICF

4. Conclusions

The jet in crossflow at Reynolds number ($Re=100$) have been performed based on the LES method, the corresponding conclusions have been listed as follows:

(1) Three-dimensional streamlines are closely related to the velocity ratios, the higher velocity ratios become, the deeper the penetration can reach. The more stable mixed vortices including the CRVP, RLV, UV, HSV and WV can be generated. The RLV will move up at the beginning, and then start to fall after a certain period of time near the nozzle of the jet.

(2) The presence of the CRVP and RLV structures can maintain quite a long distance even the flow exits at lower velocity ratio, but the RLV will be in destruction soon at larger velocity ratios under the interaction for the mixed jet in crossflow. The relative regular vortices can be generated below the CRVP and RLV under the interaction of UV and WV, which will be decomposed to a series of shocking eddy wrapped into the crossflow.

(3) The relatively symmetric vortices pair can be generated at the upper boundary. The whole vortex regions can become more circular and greater with the increasing velocity ratio.

The second vortices are also induced by the previous formed CRVP at relatively higher velocity ratios

Conflict of Interests

The authors declare that there is no conflict of interests regarding the publication of this paper.

Acknowledgment

The grant support from the National Science Foundation of China (No. U1430113) and Academic Start Program for Young Teachers of Beijing Institute of Technology (No. 3010012261502) is greatly acknowledged.

References

- Camussi R, Guj G, Stella A. (2002). Experimental study of a jet in a crossflow at very low Reynolds number. *Journal of Fluid Mechanics*, **454**: 113-144.
- Cárdenas C, Suntz R, Denev J A, et al. (2007). Two-dimensional estimation of Reynolds-fluxes and-stresses in a Jet-in-Crossflow arrangement by simultaneous 2D-LIF and PIV. *Applied physics B*, **88**: 581-591.
- Chassaing P, George J, Claria A, et al. (1974). Physical characteristics of subsonic jets in a cross-stream. *Journal of Fluid Mechanics*, **62**: 41-64.
- Chen A R, Ai H L. (2010). Computational Bridge Aerodynamics: Large Eddy Simulation. China Communications Press, Beijing. (in Chinese)
- Esmaili M, Afshari A, Jaber F A. (2015). Large-eddy simulation of turbulent mixing of a jet in cross-flow. *Journal of Engineering for Gas Turbines and Power*, **137**: 091510.
- Guan H, Wu C J. (2007). Large-eddy simulations and vortex structures of turbulent jets in crossflow. *Science in China Series G: Physics, Mechanics and Astronomy*, **50**: 118-132.
- Gutmark E J, Grinstein F F. (1999). Flow control with noncircular jets. *Annual review of fluid mechanics*, **31**: 239-272.
- Ivanova E M, Noll B E, Aigner M. (2013). A numerical study on the turbulent Schmidt numbers in a jet in crossflow. *Journal of Engineering for Gas Turbines and Power*, **135**: 011505.
- Jouhaud J C, Gicquel L Y M, Enaux B, et al. (2007). Large-eddy-simulation modeling for aerothermal predictions behind a jet in crossflow. *AIAA journal*, **45**: 2438-2447.
- Lacarelle A, Paschereit C O. (2012). Increasing the Passive Scalar Mixing Quality of Jets in Crossflow With Fluidics Actuators. *Journal of Engineering for Gas Turbines and Power*, **134**: 021503.
- Lim T T, New T H, Luo S C. (2006). Scaling of trajectories of elliptic jets in crossflow. *AIAA journal*, **44**: 3157-3160.
- Mashayek A, Behzad M, Ashgriz N. (2011). Multiple Injector Model for Primary Breakup of a Liquid Jet in Crossflow. *AIAA journal*, **49**: 2407-2420.
- Muppidi S, Mahesh K. (2007). Direct numerical simulation of round turbulent jets in crossflow. *Journal of Fluid Mechanics*, **574**: 59-84.
- New T H, Lim T T, Luo S C. (2006). Effects of jet velocity profiles on a round jet in cross-flow. *Experiments in Fluids*, **40**: 859-875..
- Saha A K, Yaragani C B. (2012). Three-dimensional numerical study of jet-in-crossflow characteristics at low Reynolds number. *Heat and Mass Transfer*, **48**: 391-411.
- Salewski M, Stankovic D, Fuchs L. (2008). Mixing in circular and non-circular jets in crossflow. *Flow, Turbulence and Combustion*, **80**: 255-283.
- Srinivasan S, Pasumarti R, Menon S. (2012). Large-eddy simulation of pulsed high-speed subsonic jets in a turbulent crossflow. *Journal of Turbulence*, **13**: N1.
- Yuan L L, Street R L, Ferziger J H. (1999). Large-eddy simulations of a round jet in crossflow. *Journal of Fluid Mechanics*, **379**: 71-104.